communications biology

A Nature Portfolio journal

Article

https://doi.org/10.1038/s42003-025-07728-2

High hydrostatic pressure stimulates n-C_{16} mineralization to CO_2 by deep-ocean bacterium *Alcanivorax xenomutans* A28

Check for updates

Huaying Lin[1], Yongxin Lv[1] & Yu Zhang[1,2]

Medium-chain alkanes have strong ecological impacts on marine ecosystems due to their persistence, toxicity, and ability to travel long distances. Microbial degradation is the dominant and ultimate removal process for n-alkanes in the deep ocean, where high hydrostatic pressure (HHP) regulates microbial activity. To gain insight into the impact of hydrostatic pressure (HP) on n-alkane degradation, we applied the deep-ocean experimental simulation to culture *Alcanivorax xenomutans* A28, a novel piezotolerant bacterium strain from trench sediment, with n-C_{16} as the sole carbon source under different HPs (0.1, 40, and 80 MPa). Activity analysis demonstrated that HHP stimulated the n-C_{16} complete mineralization ratio. Transcriptomic and metabolomic analyses showed that HHP induced the intracellular oxidative stress and accelerated the tricarboxylic acid (TCA) cycle. These results indicate a shift of n-alkanes biodegradation pattern regulated by HP, elucidating the fate and ecological risk of n-alkanes in the deep ocean.

N-alkanes, one of the main components of petroleum, enter into marine environment through natural seep and human activites[1]. It has a strong ecological impact on the marine ecosystem because of its persistence[2], potential for bioaccumulation and toxicity[3], and ability to travel long distances with marine snow and particles[4,5], even down to the bottom of the Mariana Trench at the water depth of 10,500 m[6,7].

When the ocean ecosystem is exposed to emergency oil spills, microbial degradation is the dominant and ultimate natural removal process for n-alkanes. At the surface ocean, the canonical microbial n-alkane degradation normally begins with an activation reaction that introduces oxygen-containing functional groups. This step is typically mediated by hydroxylases and requires energy to overcome the chemical inertness, which is the initial and rate-limiting step in the n-alkanes degradation[8,9]. There are several hydroxylase systems responsible for the activation of different length of chain n-alkane. For example, soluble cytochrome P450s and integral membrane non-heme iron monooxygenases AlkBs predominately participate in the activation of n-alkane with chain length ranging from 5 to 17 carbons[10]. The putative flavin-binding monooxygenase AlmA of the genus *Alcanivorax* functions as the hydroxylase for n-alkane with chain length ranging from 22 to 36 carbons[10,11]. The oxidation step is related to electron transport and intracellular oxidative status. In the AlkB-type system, reductase (AlkT) and hemoglobin reductase (AlkG) are responsible for transferring two electrons from NADH to AlkB[12]. The intermediate fatty alcohols are subsequently oxidized into fatty aldehydes and fatty acids by dehydrogenase and then enter the β-oxidation and tricarboxylic acid (TCA) cycle for energy metabolism[13].

In the deep ocean (> 1000 m water depth), the microbial degradation of n-alkanes is regulated by high hydrostatic pressure (HHP), and therefore reveals distinct patterns compared with that at surface ocean. At the cellular level, HHP can induce intracellular oxygen stress[14], leading to a shift in anabolism (biomass synthesis) and catabolism (CO_2 production, etc.), and altering the n-alkanes degradation efficiency and pathway in deep ocean as what have been reported from both in situ investigations and laboratory cultivations[15–18]. For example, in the cultivation of a deep sea sediment sample, the TCA cycle rate under 30 MPa can rarely meet high energy demand, resulting in a slow degradation of long-chain n-alkane[17]. In *Marinobacter hydrocarbonoclasticus* strain #5, HHP (35 MPa) had no impact on n-hexadecane(n-C_{16}) degradation but inhibited the synthesis of n-hexadecane-derived wax esters that accumulated in the cells as individual lipid bodies[19]. Moreover, HHP has a selective impact on the dominant taxa

[1]School of Oceanography; Shanghai Key Laboratory of Polar Life and Environment Sciences; Key Laboratory of Polar Ecosystem and Climate Change, Ministry of Education; Shanghai Frontiers Science Center of Polar Science, Shanghai Jiao Tong University, Shanghai, China. [2]Yazhou Bay Institute of Deepsea Sci-Tech, Shanghai Jiao Tong University, Sanya, China. e-mail: zhang.yusjtu@sjtu.edu.cn

of alkane degraders. Among all the identified alkane degraders, the genus *Alcanivorax* is the most widely distributed in the deep oceans, indicating its adaptation to HHP[6,20]. Laboratory enrichment under HHP also showed *Alcanivorax* was selectively enriched with n-alkane addition, indicating its competitive edge in the deep ocean[7,21].

However, studies on the effect of hydrostatic pressure (HP) on the n-alkane biodegradation is affected by HP, in terms of its conversion fate, remain scarce primarily because of two limitations: (1) lack of ability to simulate extreme HHP in the deep ocean in the laboratory, resulting in the inability to HHP cultivation and detection; (2) lack of n-alkane-degrading bacteria that can grow under extreme HHP, resulting in no suitable biomaterial for research. In this study, we used *Alcanivorax xenomutans* A28, a piezotolerant strain with n-alkane degradation capacity isolated from 7663.5 m of deep-ocean sediments, for culture experiments under different HPs (0.1, 40, and 80 MPa) and at 4 °C in specially designed high-pressure incubation vessels. Chemical parameters, transcriptomics, and metabolomics were used to evaluate the microbial utilization of n-C_{16} and the degradation process of this strain under different HPs. This study enhances our understanding of the microbial degradation efficiency and mechanisms of n-alkanes and provides certain basic knowledge to assist the deep-ocean petroleum remediation.

Results

General characteristics of *Alcanivorax xenomutans* A28

The commonly known n-alkane-degrading genus *Alcanivorax* was abundant (from approximately 1.00% to 21.02% in the first 16 cm and 1.42% in the 0–2 cm layer) in the in situ sediment (Supplementary Fig. 1). A piezotolerant bacterium strain *Alcanivorax xenomutans* A28 was isolated from 0 to 2 cm sediment layer. Strain A28 was taxonomically affiliated with the family *Alcanivoracaceae*, genus *Alcanivorax*. 16S rRNA gene sequence analysis revealed 99.93% and 99.86% sequence similarity with *Alcanivorax xenomutans* JC109 and *Alcanivorax dieselolei* B5, respectively (Fig. 1A). Based on genomic average nucleotide identity (ANI), it exhibited 98.52% and 93.62% similarity with A. *xenomutans* JC109 and A. *dieselolei*, respectively. The complete genome consists of one chromosome with a total length of 4,710,204 base pairs (bp) with a G + C content of 61.44% (Fig. 1B; Supplementary Table 1). Strain A28 possess two 16S rRNA gene copies in its genome.

Genomic analysis suggested the n-alkanes degradation capacity of A. *xenomutans* A28. The genome harbored three types of n-alkane hydroxylase systems, cytochrome P450s (chr_2087 and chr_2372), the non-heme diiron integral membrane n-alkane monooxygenase genes *alkB* (chr_102, chr_700, and chr_4245), and the flavin-binding monooxygenase gene *almA* (chr_2065). The genes of two enzymes participating in electron transfer to AlkB, rubredoxin reductase gene *alkT* (chr_4201) and the rubredoxin *alkG* (chr_4202) were also annotated in genome (Table S2). The *almA* sequence of strain A28 showed 100% similarity with the amino acid sequence of *almA* from A. *dieselolei* B5 (Supplementary Fig. 2).

Degradation performance of *Alcanivorax xenomutans* A28 for n-hexadecane under different HPs

We incubated *Alcanivorax xenomutans* A28 in artificial seawater with and without n-C_{16} as the sole carbon source under different HPs (0.1, 40, and 80 MPa) at 4 °C. The growth of strain A28 was supported by the addition of n-C_{16} but minimally impacted by HP (Fig. 2; Supplementary Fig. 3). The cell numbers significantly increased with n-C_{16} compared to those without n-C_{16} (one-tailed T test, $p < 0.05$). Additionally, no significant differences in cell numbers were detected among the three HPs incubations (ANOVA analysis, $p < 0.05$). The cells under 0.1 MPa had a higher protein content than those under 40 and 80 MPa (Supplementary Fig. 4).

To test the biodegradation performance of strain A28 for n-C_{16} under different HPs, we quantified the n-C_{16} consumption rate, amount of CO_2 production, and the complete mineralization ratio (amount of carbon of CO_2 production to n-C_{16} consumption). HHP (40 and 80 MPa) inhibited

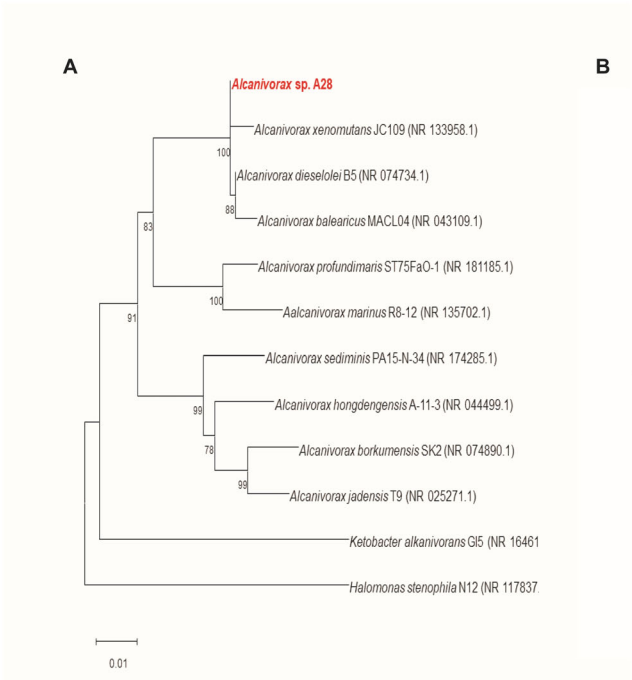

Fig. 1 | Genetic tree based on 16S rRNA gene and circular genome of *Alcanivorax xenomutans* strain A28. A Phylogenetic tree based on 16S rRNA gene sequences showing the relationship of strain A28 within the genus *Alcanivorax*. The tree was reconstructed by the Neighbor-Joining method and rooted by using *Ketobacter alkanivorans* GI5 and *Halomonas stenophila* N12 that belong to the family Alcanivoracaceae as the outgroups. Numbers at nodes are the percentage of bootstrap support (based on 1000 replications). GenBank accession numbers for 16S rRNA gene sequences are shown in parentheses. Bar indicates 1 nucleotide substitution per 100 nt. **B** Circular representation of *Alcanivorax xenomutans* A28 genome. From the inside to the outside, the first circle represents the scale; The second circle represents GC Skew; The third circle represents the GC content; The fourth and seventh circles represent the COG (Cluster of Orthologous Groups of proteins) to which each CDS (Coding Sequence) belongs; The fifth and sixth circles represent the position of CDS, tRNA and rRNA on the genome.

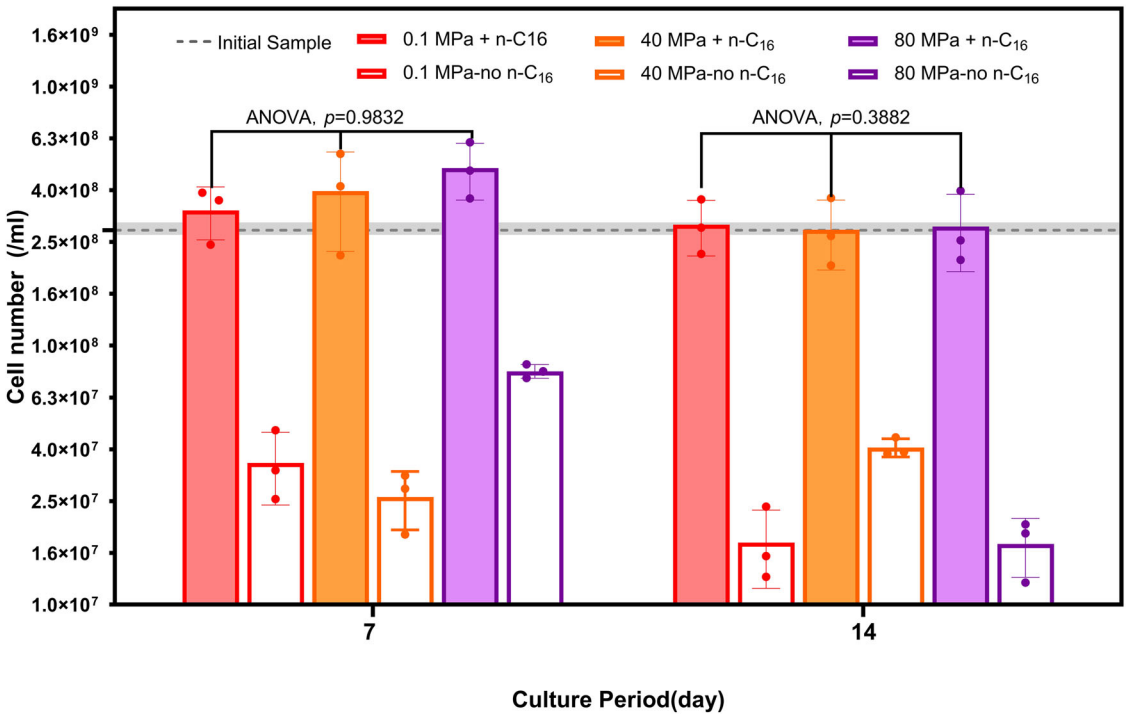

Fig. 2 | Cell number on day 7 and 14 under different HPs (0.1 MPa, 40 MPa, and 80 MPa). The statistical significance analysis among three HPs with n-C_{16} addition was conducted by one-way ANOVA. Error bars represent standard deviation of three biological replicates under the same treatment.

n-C_{16} degradation (Fig. 3). After two weeks of incubation, the total removal of n-C_{16} reached 20%, 15%, and 11% under 0.1, 40, and 80 MPa, respectively. The calculated consumption rates based on the slopes of the trend lines were 0.46, 0.35, and 0.30 mg n-C_{16} per day under 0.1, 40, and 80 MPa, respectively. n-C_{16} consumption decreased with HP elevation, while CO_2 production increased, resulting in a higher complete mineralization ratio under 40 and 80 MPa than that under 0.1 MPa (Fig. 3). The incubation under 80 MPa showed lower n-C_{16} consumption rate but higher CO_2 production proportion compared with those under 0.1 and 40 MPa. The averaged mineralization ratios (calculated from four sampling points, see the details in Methods) ranged from 0.0039 ± 0.0013‰ (mean ± s.d.), 0.0059 ± 0.0012‰, and 0.0090 ± 0.0012‰ under 0.1, 40, and 80 MPa, respectively. This pattern was consistent with the pH changes caused by CO_2 production (Supplementary Fig. 5).

Cellular metabolism of n-hexadecane oxygenation under different HPs

Using transcriptome and metabolome analyses, we examined throughout the n-alkane degradation pathway of strain A28 and focused on n-alkane oxygenation steps. The n-alkane hydroxylases were downregulated under 40 and 80 MPa compared with those under 0.1 MPa (Fig. 4; Supplementary Table 2). Among the three types of n-alkane-degrading enzyme genes, *alkB* was the most severely affected at the transcriptional level under HHP. The expression of *alkB* in chr_700 was significantly downregulated under 80 MPa (log_2 FC: −2.07 on day 7) and 40 MPa (log_2 FC: −4.57 on day 7 and −2.96 on day 14). In addition, two other genes of AlkB-depending enzymes, *alkG* and *alkT*, were also significantly downregulated under HHP. In particular, *alkG* was significantly downregulated both on day 7 and 14 under 80 MPa than that under 0.1 MPa. The putative *almA* was significantly upregulated under 40 MPa, with 1.48 log_2 FC on day 7 and 1.17 on day 14 (Fig. 4; Supplementary Table 2).

Conversion of the aldehyde into fatty acid during n-alkane oxygenation is carried out by alcohol dehydrogenases (ADHs) and aldehyde dehydrogenases (ALDHs). We identified five ADH homologues (chr_245, chr_405, chr_1636, chr_2506, and chr_2884) and two ALDH homologues (chr_1622 and chr_4234) in strain A28 genome. Among the five ADH homologues, the ADH homologues chr_405 and chr_245 were significantly upregulated under 40 MPa, and chr_245 was only upregulated under 80 MPa, compared with those under 0.1 MPa (Fig. 4). Both two ALDH homologues, chr_1622 and chr_4234, were only significantly upregulated under 80 MPa, whereas they were unaffected under 40 MPa, compared with those under 0.1 MPa.

Using metabolome analysis, we identified the potential hexadecane intermediates produced during n-alkane oxygenation. The final oxidation product hexadecenoic acid showed no significant differences among the three HPs, indicating that the net production of hexadecenoic acid was unaffected by HP (Fig. 5A). Lipid-related products, such as PG (16:1(9Z)-16:0), PE (34:2), PE (20:1(11Z)-14:1(9Z)) showed higher concentrations under 0.1 MPa than HHP (ANOVA, $p < 0.01$; Supplementary Fig. 6).

Energy metabolism under different HPs

In the initial step of β-oxidation, seven long-chain acyl-CoA synthetase homologues were identified in strain A28 (chr_1199, chr_1604, chr_2040, chr_2190, chr_1909, chr_3554, and chr_3666). The gene expressions of long-chain acyl-CoA synthetases were generally upregulated under HHP. Gene chr_1199 was significantly upregulated under both 40 MPa (day 14) and 80 MPa (day 7 and 14), and chr_3666 was significantly upregulated under 80 MPa (day 7 and 14). Gene chr_1604 was significantly upregulated under 40 MPa (day 14). No significant differences were observed in the expression of chr_2040 and chr_2909. Among the seven long-chain acyl-CoA synthetase homologues, chr_2190 was the only one that was significantly downregulated under 80 MPa (log_2FC = -1.21 on day 7 and -1.42 on day 14, adjusted $p < 0.05$) compared with that under 0.1 MPa.

For other steps of β-oxidation and the entire TCA cycle, 25 of 39 genes were significantly upregulated and no gene was significantly downregulated under 80 MPa; whereas, 9 of 39 genes were significantly upregulated and 15 of 39 genes were significantly downregulated under 40 MPa (Fig. 4). Sixteen genes were significantly differentially expressed both under 40 MPa and 80 MPa, compared with those under 0.1 MPa. These 16 genes were all significantly upregulated under 80 MPa and 11 genes were downregulated under 40 MPa, compared with those under 0.1 MPa.

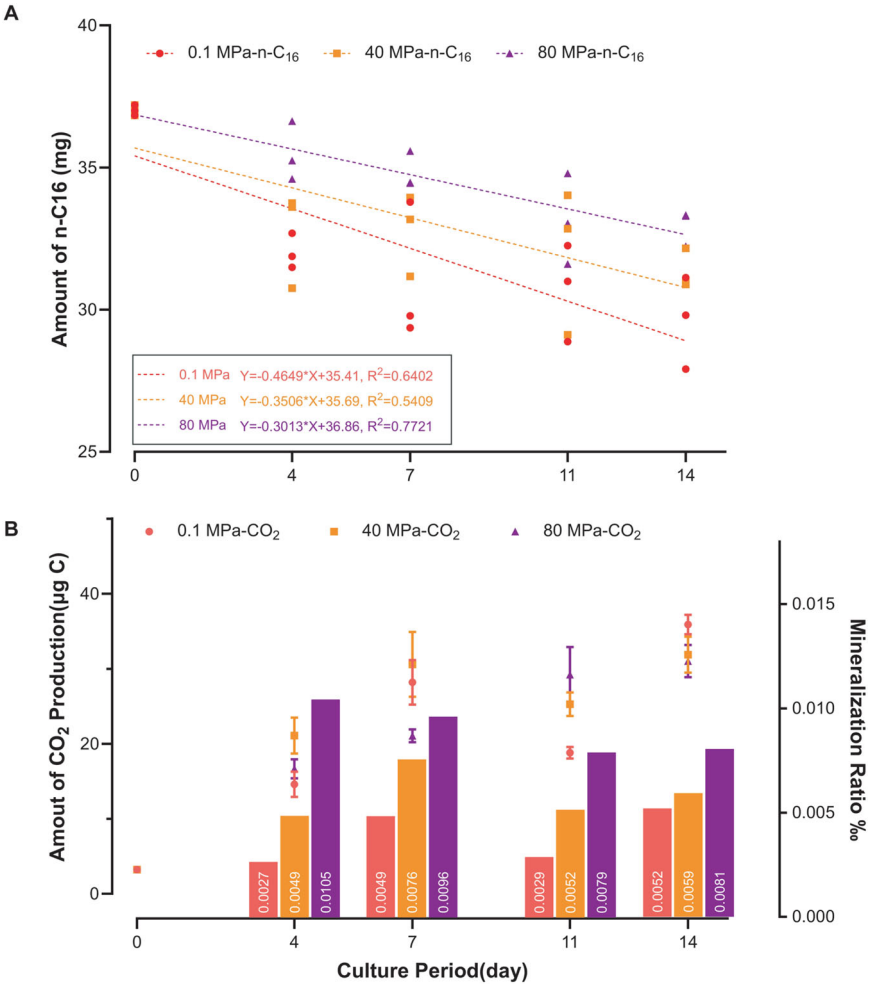

Fig. 3 | Amount of n-C_{16} consumption, CO_2 production and mineralization ratio by strain A28 under different HPs (0.1, 40, and 80 MPa). **A** Amount of n-C_{16} consumption under different HPs (0.1, 40, and 80 MPa). The dotted lines are the fitting lines by simple liner regression and the grey box shows the fitting slope and goodness of fit. **B** The CO_2 production and mineralization ratio based on the amount of carbon of n-C_{16} consumption to CO_2 production under different HPs. Error bars represent standard deviations of three biological replicates under the same HP.

In the TCA cycle, HHP stimulated all the genes related to two CO_2-producing steps. In the reaction from isocitrate to α-ketoglutarate, two isocitrate dehydrogenase homologues (chr_687 and chr_1990) were significantly upregulated under 40 MPa ($log_2FC > 1.67$, adjusted $p < 0.05$) and 80 MPa ($log_2FC > 1.08$, adjusted $p < 0.05$), compared with that under 0.1 MPa. For the step from α-ketoglutarate to succinyl-CoA, α-ketoglutarate dehydrogenase homologues (chr_2681, chr_2682, and chr_2683) were upregulated under 80 MPa ($log_2FC > 1.18$, adjusted $p < 0.05$) while downregulated under 40 MPa ($log_2FC < -1.46$, adjusted $p < 0.05$), compared with those under 0.1 MPa. On the contrary, the expression of glyoxylate shunt (GS) related genes (chr_3263 and chr_1968) was significantly downregulated under 40 MPa (chr_3263: $log_2FC < -1.82$, adjusted $p < 0.05$; chr_1968: $log_2FC = -1.14$, adjusted $p < 0.05$ on day 7) and only malate synthase homologues chr_1969 was upregulated under 80 MPa. Three identified TCA-related intermediates, citrate, cis-Aconitase, and succinyl-CoA, all had minimum concentrations under 80 MPa among the three HPs except for succinyl-CoA on day 7 (Fig. 5B–D). Besides, the expression levels of homologous involved in oxidative phosphorylation machinery, such as ATP synthase, succinate dehydrogenase, cytochrome bc complex, and cytochrome bd complex, were significantly upregulated under 80 MPa (Supplementary Fig. 7). This further indicated the intensified energy metabolism during n-alkane biodegradation under elevated HPs.

Oxidative stress level of *Alcanivorax xenomutans* A28 under different HPs

HHP triggered a higher reactive oxygen species (ROS) production and upregulated antioxidant related genes (Fig. 6). Intracellular H_2O_2 accumulated with incubation time. The concentration of intracellular H_2O_2 between the incubation under 0.1 MPa and 40 MPa was closely similar in the first three sampling points ($p = 0.1163$, paired T test) and the largest difference reached 2.98×10^{-8} μM per cell at the last sampling point day 14. Among the three HPs, the concentration of intracellular H_2O_2 under 80 MPa was higher than those under 0.1 and 40 MPa (except for day 4). The total antioxidant capacity quantified by the ferric reducing ability of the plasma (FRAP) method showed the cells under HHP possessed similar levels of total antioxidant capability (one-way ANOVA analysis, $F(1.182, 3.545) = 0.5880$, $p = 0.5189$; Fig. 6B).

For the genes related to antioxidant system, an overall up-regulation under HHP was observed (Fig. 6C). The *sod1* gene (chr_3251), encoding for enzyme that participates in O_2^- removal to H_2O_2, was significantly upregulated under 40 MPa ($log_2FC = 2.24$ on day 7 and 2.49 on day 14, adjusted $p < 0.05$) and 80 MPa ($log_2FC = 1.03$ on day 7 and 1.99 on day 14, adjusted $p < 0.05$), comparted with that under 0.1 MPa. The *ahpC* gene (chr_3156), encoding for enzyme that directly participates in H_2O_2 removal, was also significantly upregulated under 40 MPa ($log_2FC = 1.44$ on day 7 and 2.46 on day 14, adjusted $p < 0.05$) and 80 MPa ($log_2FC = 1.39$ on day 7, adjusted $p < 0.05$). The *trxB* gene(chr_1998), encoding for thioredoxin reductase that provides electrons to thiol-dependent peroxidases, was significantly upregulated under 40 MPa ($log_2FC = 3.09$ on day 7 and 1.23 on day 14, adjusted $p < 0.05$). Additionally, higher gene expression levels of *trxB*, *ahpC* and *sod1* were observed under 40 MPa than those under 80 MPa.

Discussion

HHP slows down the microbial degradation of n-hexadecane by inhibiting the oxygenation of n-alkane

In this study, the effect of HP on n-C_{16} degradation was observed up to 80 MPa and HHP negatively affected the degradation of n-C_{16}. This is consistent with the results of previous studies conducted under lower HP

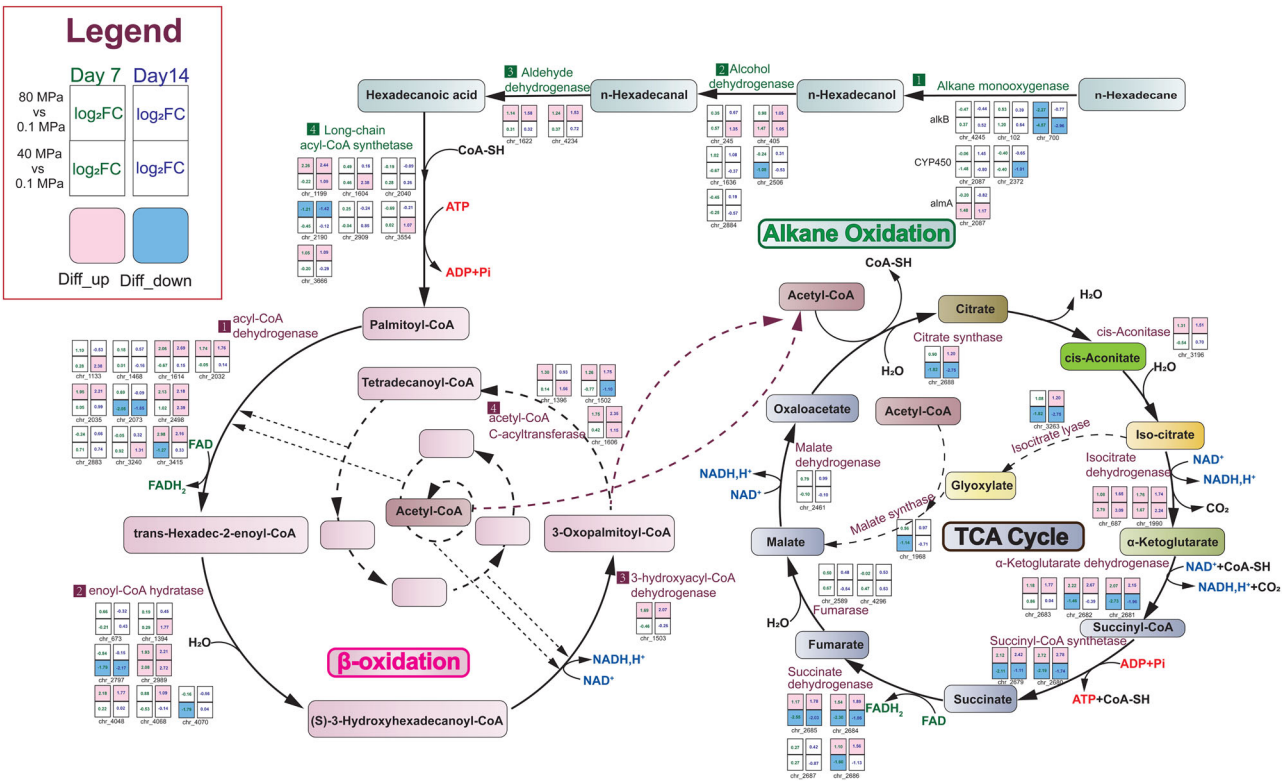

Fig. 4 | Transcriptional profiles of key genes related to n-alkane oxidation pathway, β-oxidation of fatty acid and the TCA cycle in strain A28 under different HPs (0.1, 40, and 80 MPa). Arrows represent direction of biochemical reactions. The number in the block represents the Log_2FC of gene expression under HHP (40 or 80 MPa) compared with that under 0.1 MPa. Color of number indicates different sampling points that green represents the day 7 and purple represents the day 14. Block with pink or blue color indicates the transcriptional level of differentially expressed genes compared with that under 0.1 MPa. Pink block indicates significantly upregulation ($Log_2FC \geq 1$, adjusted p value < 0.05) while blue block indicates significantly downregulation ($Log_2FC \leq -1$, adjusted p value < 0.05). Each transcriptional analysis involved three biological replicates under the same HP.

levels. Both laboratory cultures and field investigations have indicated that HHP (10 and 20 MPa) or water depth (down to 4000 m water depth where the HP is approximately 40 MPa) can inhibit the degradation of organic carbon such as n-alkanes by microorganisms (especially piezotolerant microorganisms)[17,22]. Furthermore, our findings indicate that HHP inhibits the rate of n-alkane degradation. This led to the discovery that oil pollutants, such as n-alkanes, undergo slower biodegradation when sinking into the deep ocean than those in the surface ocean. Additionally, a higher proportion of long-chain n-alkane (> C_{26}) preserved during the four years following the Mexico oil spill accident[15]. Our study further confirms the important role of HP in deep-ocean n-alkane degradation.

Previous studies indicated the inhibited heterotrophic activity by HHP may be related to a decreased growth rate[17,22]. In this study, no significant impact from HHP was observed on the growth rate of strain A28 (Fig. 2). This indicates that HHP inhibits the n-alkane degradation rate by regulating intracellular processes rather than by controlling the population size. Using transcriptome and metabolome analyses, we found that the oxygenation of n-alkane was the potential bottleneck for n-C_{16} consumption under HHPs. The n-alkane oxygenation is generally the initial and rate-limiting step in aerobic n-alkane degradation, as n-alkane-activating enzymes must overcome the low chemical reactivity of n-alkanes[13]. It is catalyzed by n-alkane hydroxylases. Strain A28 has three n-alkane hydroxylase systems (AlkB, putative AlmA and cytochrome P450). These n-alkane hydroxylases have different substrate utilization ranges or induction patterns[4].The enzymes AlkB and cytochrome P450 primarily degrade short- and medium-chain n-alkane (C_5-C_{17})[10,11], while AlmA is more involved in the degradation of longer chain n-alkane (>22 C)[11]. AlkB-type n-alkane hydroxylases exhibit greater affinities for C_8-C_{20} substrates than cytochrome P450[23], and were the most transcriptionally sensitive n-alkane hydroxylases under HHP in this study (Fig. 4; Supplementary Table 2). The enzyme AlkB is a class of non-heme diiron enzyme whose activation requires the transfer of two electrons from NADH via reductase AlkT and hemoglobin reductase AlkG[12]. The downregulation of *alkB* and *alkG* further suggests that the AlkB system was generally inhibited by HHP and may limit the oxygenation rate for n-C_{16} (Fig. 4; Supplementary Table 2). The inhibitory effect of HHP on n-alkane hydroxylase gene *alkB* has been reported in a few studies, the underlying mechanism remains underexplored[24]. The accumulation of ROS, such as H_2O_2, inhibits the activation of n-alkane oxygenases[25]. Based on our results, we propose that the function of AlkB was inhibited by the high ROS level, induced by HHP incubation (Fig. 6).

Notably, the n-alkane degradation rate was higher under 40 MPa than that under 80 MPa despite the observed downregulation of *alkB* gene expression. This discrepancy suggests that potential isozymes of AlkB may be functioning, e.g. AlmA[26]. The AlmA in strain A28 shares 100% sequence similarity with AlmA in A. *dieselolei* B5 (Supplementary Fig. 2); the latter has been proven to degrade n-C_{16} based on enzymatic activity assay[27]. The *almA* was significantly upregulated under 40 MPa compared with that under 0.1 and 80 MPa (Fig. 4; Supplementary Table 2). The unusually high expression of *almA* under 40 MPa when degrading n-C_{16} may help to offset the inhibition of *alkB* by HHP, resulting in a slightly higher degradation rate of n-C_{16} than that under 80 MPa. The high expression level of *almA* suggests its functioning advantage under HHP. The enzyme AlmA is a class of flavin-dependent enzymes. Due to the low electrophilicity, flavin-dependent enzymes often have a low sensitivity to H_2O_2, and can even directly eliminate H_2O_2 in some cases[25]. As shown in our results, the expression level of *almA* in deed has the similar trend as the H_2O_2 level (Fig. 6A). However, since the function of the AlmA-type hydroxylase involved is far from well

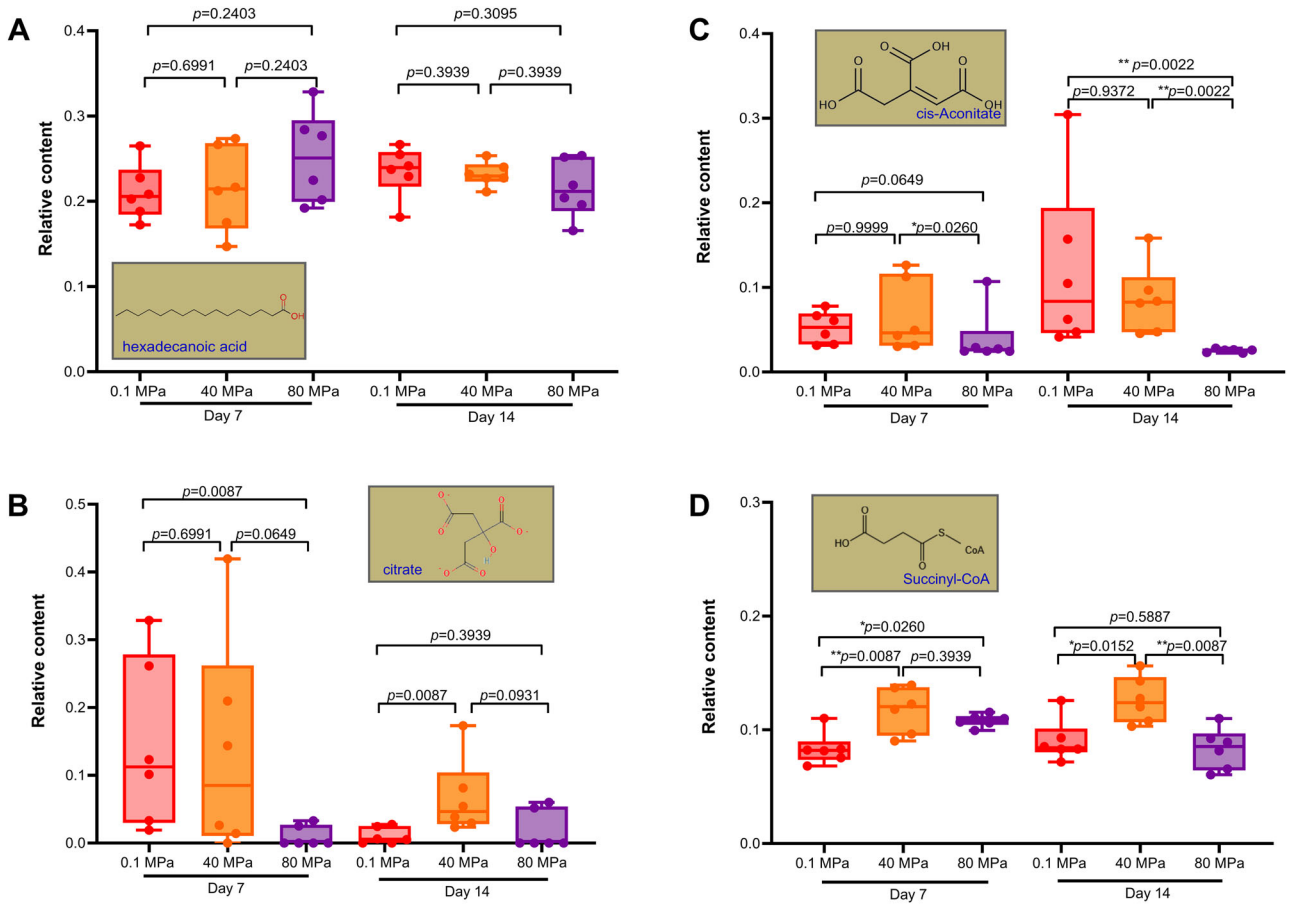

Fig. 5 | Relative content of potential metabolites in n-C_{16} degradation. Relative content of potential hexadecane-derived metabolites (**A**) and TCA cycle related intermediate (**B**, **C**, **D**). The relative content was the peak area normalized to total peak area. The significant analysis was conducted by unpaired and two-tailed T test. Box plots indicate upper and lower quartiles (top and bottom of the box), median (line within box), and the dot represents the value of each biological replicate. Error bars represent standard deviation of six replicates under the same HP.

understood, the relationship between its expression with HPs needs to be further investigated.

HHP accelerates the complete mineralization process of microbial n-hexadecane degradation by stimulating energy metabolism

The ratio of CO_2 production to n-C_{16} consumption increased with HP elevation, despite the decrease in n-C_{16} degradation rate (Fig. 3). This suggests that HHP stimulates the complete mineralization of n-C_{16}. Previous studies generally assumed that high CO_2 production may be indicative of a high degradation rate of organic carbon[28]. However, whether this relationship remains stable under different HPs has yet to be investigated. Herein, we demonstrated the lack of a positive correlation between the amount of CO_2 production and n-C_{16} consumption under different HPs (Fig. 3). It should be noted that since a sacrificial sampling method was used (see the details in Material and Method), biological batch effects between samples were inevitably introduced, which prevented us from calculating the carbon balance through cultivation periods. Therefore, we could only compare the CO_2 accumulation at the same time point among different HPs. Nevertheless, the observed phenomenon also indicates that the removal of same amount of n-alkanes will generate more CO_2 in deeper ocean environments.

The n-alkanes are used by microorganisms for anabolism (composition of biomass) and catabolism (production of CO_2, etc.)[8]. The varying ratios of CO_2 production to n-C_{16} consumption indicates that HHP changes the allocation of n-alkanes for anabolism and catabolism. That is, the proportion of n-C_{16} for catabolism increased under HHP, whereas that for anabolism decreased. Through the metabolomic analysis, we identified several metabolites involving in the construction of cell structures and membranes that were significantly depleted under 80 MPa (Supplementary Fig. 6). Additionally, the culture under 0.1 MPa exhibited a higher cellular protein content than that under HHP (Supplementary Fig. 4). These results further suggests that biomass synthesis is weakened under HHP. For example, hexadecenoic acid serves as substrates for biosynthesis, and an intensified biosynthesis process would cause less accumulation of hexadecenoic acid under 0.1 MPa. This explains why the cells under HHP consumed less n-C_{16} and transferred a higher proportion to CO_2 but still accumulated same levels of hexadecenoic acid as those under 0.1 MPa (Fig. 5A).

For catabolism, n-C_{16} is completely degraded through β-oxidation and the TCA cycle, where CO_2 is the final product. The complete oxidation of 1 mole n-C_{16} to CO_2 can contribute a net reducing power of 106 mole ATP, 31 mole NADH and 14 mole $FADH_2$, contributing to high energy and reducing power[29]. The expression of genes associated with β-oxidation and the TCA cycle were upregulated under 80 MPa, indicating that HHP stimulated catabolism (Fig. 4). The low intracellular concentrations of the relevant intermediate metabolites under HHP also further supported the high cycling rate of the TCA cycle (Fig. 5B–D). In particular, CO_2 production through the TCA cycle under HHP was significantly upregulated compared with that under 0.1 MPa (Fig. 5). The glyoxylate shunt, which is generally activated during alkane degradation, was downregulated overall under 40 MPa and unaffected under 80 MPa (Fig. 4). The glyoxylate shunt can bypass the TCA cycle, contributing to less CO_2 and NADH/$FADH_2$[30]. Upregulation of CO_2-producing genes in the TCA cycle and avoidance of

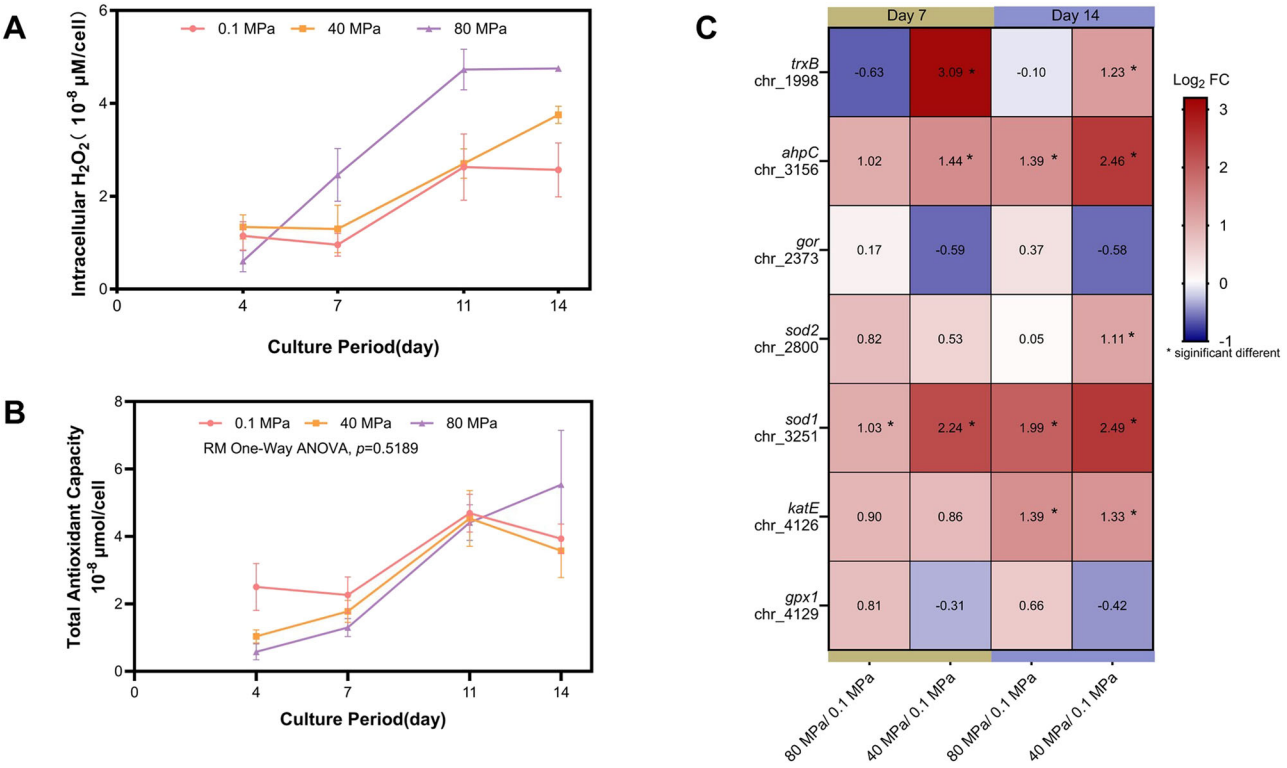

Fig. 6 | Oxidative stress response of *Alcanivorax xenomutans* A28 under different HPs (0.1 MPa, 40 MPa, and 80 MPa). A The concentration of intracellular H_2O_2. The concentration was normalized to cell number. **B** Total antioxidant capacity by the FRAP method. The total antioxidant capacity is expressed as the concentration of the $FeSO_4$ standard solution. The concentration was normalized to cell number. The RM (repeated measured) One-Way ANOVA was conducted among three HPs. Error bars (**A**, **B**) represent standard deviation of three biological replicates under the same HP. **C** Transcriptional heat map of key genes related to antioxidant system. The number inside box indicates the value of $\log_2$ FC in the transcriptional comparison. The asterisk (*) indicates the transcriptional level gene is significantly differentially expressed with |log2 FC|≥ 1 and adjusted *p*-value < 0.05.

glyoxylate shunt contribute to a high rate of n-C_{16} mineralization to CO_2. This may be related to the increased energy demand under HHP, which is evidenced by the upregulation of genes involved in oxidative phosphorylation for ATP synthesis under 80 MPa (Supplementary Fig. 7). This is consistent with the theory that the upregulation of energy metabolism is a common strategy to cope with oxidative stress induced by HHP[31,32]. Previous studies found that *Halomonas titanicae* ANRCS81 suffered an increased oxidative stress when cultivated under 40 MPa compared to that under 0.1 MPa, accompanied by the upregulation of TCA cycle-related genes[32]. This is consistent with the elevated H_2O_2 and the upregulation of antioxidant enzyme genes including *sod1*, *ahpC* (Fig. 6). Thus, enhanced HP promotes the catabolism of n-C_{16} under HHP.

Summary

In this study, we reported the regulatory mechanism of a piezotolerant strain *Alcanivorax xenomutans* A28 for n-C_{16} biodegradation up to 80 MPa. We found that HHP significantly inhibited the oxygenation of n-alkane by inducing intracellular oxidative stress, leading to a reduced n-alkane degradation rate. The high oxidative stress under HHP also accelerated the complete oxidation of n-alkane, resulting in a high mineralization ratio. These findings greatly enhanced our understanding for the natural capacity of n-alkanes bioremediation and the fate of n-alkanes at different water depths. This study provides a new perspective on ecological risk evaluation for deep-ocean n-alkane and oil pollution.

Methods

Isolation for Alcanivorax xenomutans A28

The surface sediment was collected from the West Philippine Basin (16°57'22" N, 129°44'38"E) at a depth of 7663.5 m by the lander "Fendouzhe" aboard the R/V *TAN SUO YI HAO* during cruise TS-21 in August 2021. The sediment was sliced into 2 cm intervals and preserved in sample bags (B00992, Whirl-Pak, USA) at 4 °C. The surface sediment (0–2 cm) was first incubated in the ONR7a medium[33] supplemented with n-C_{16} and n-C_{18} addition (Sigma-Aldrich, USA) under ambient pressure, 4 °C. After two weeks of cultivation, the supernatant was spread on the ONR7a solid plate[33] with n-C_{16} and n-C_{18} addition. A single colony was picked out and streaked onto a solid ONR7a plate. After repeated streaking, the pure strain was isolated and identified as *Alcanivorax xenomutans* based genomic analysis. Details on DNA extraction for genome analysis is described in the Supplementary Methods.

Microbial analyses

Culture under different HPs. To harvest sufficient cells for incubation under different HPs, strain A28 was first cultured in ONR7a medium with n-C_{16} addition under 25 °C, 0.1 MPa. About 5 L cultures with an OD_{600} of approximately 0.53 (about 5×10^8 cells per ml) were centrifuged at 3000 rpm for 10 min at 4 °C to harvest cell pellet. The pellet was washed twice by ONR7a medium to remove organic carbon. Cells were then resuspended in 7 L ONR7a medium. The cell suspensions were divided into 50-ml syringes (Kindly, China) without any headspace, in which 50 μl n-C_{16} (8.20633, Sigma-Aldrich, USA) was supplied as the sole carbon source. The syringes were cultured separately under atmospheric pressure (0.1 MPa) and in high-pressure vessels (HPK03, Shanghai Jiao Tong University, China; Supplementary Fig. 8) with 40 MPa and 80 MPa at 4 °C.

Before pressurization, all cultures in syringes were precultured under 0.1 MPa, 4 °C for 12 h to adapt low temperature conditions. The time at which culture syringes were transferred into the high-pressure vessels was considered T_0. Culture syringes were sampled on days 4, 7, 11, and 14. Two blank control groups (cell suspension without n-C_{16} and sterile ONR7a

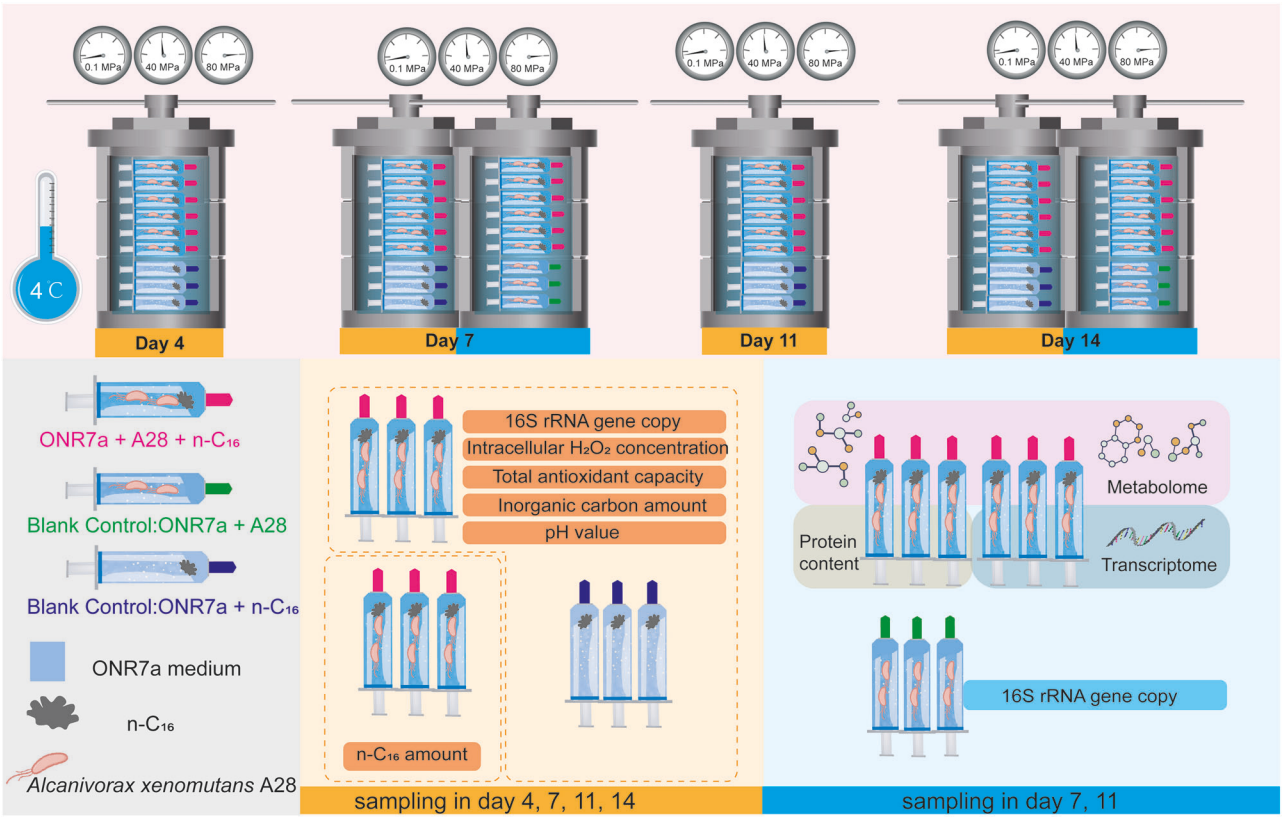

Fig. 7 | The schematic diagram of the experimental procedure in this study. The strain A28 was incubated under three HPs, 4 °C. Only the sample for omics analysis were sampled on day 7 and 14. The schematic diagram was created by the authors using Adobe Illustrator.

medium with n-C_{16}) were also set up and tested under 0.1, 40, and 80 MPa. The detailed experimental procedure is illustrated in Fig. 7.

Bacterial growth monitoring. To evaluate the bacterial growth, quantitative real-time PCR for 16S rRNA gene was used to monitor growth. DNA was extracted with a Bacterial Genomic DNA Extraction Kit (DP302, Tiangen, China). The primer pair 341f-519r (341F: 5′-CCTACGGGWGGCWGCA-3′ and 519R: 5′-TTACCGCGGCKGCTG-3′), which is specific to the 16S rRNA gene, was used for quantitative real-time PCR. According to the manufacturer's instructions for PowerUp™ SYBR™ Green Master Mix (A25742, Thermo Fisher, USA), quantitative real-time PCR was performed on the Real-Time PCR System (QuantStudio 5, Applied Biosystems, USA) with a standard two-step amplification program. The blank control group without n-C_{16} was sampled for 16S rRNA gene copy number detection only on day 7 and 14. Cells from a 25 mL culture on day 7 and 14 were centrifuged at 10,000 × *g* for 5 min at 4 °C for protein extraction and quantification (Supplementary Methods).

Intracellular H_2O_2. Intracellular H_2O_2 was measured using a Hydrogen Peroxide Assay Kit (S0038, Beyotime, China) to assess the oxidative response of the cells. Approximately 2 ml of culture was centrifuged at 10,000 × *g* for 3 min at 4 °C to collect the cell pellet. The cell pellet was resuspended a the cell lysis buffer and subjected to ultrasonication and centrifugation. The resulting supernatant was used for intracellular H_2O_2 measurement with lysis buffer as the diluent in standard sample preparation. Intracellular H_2O_2 level was normalized to the cell number.

Total antioxidant capacity. Total antioxidant capacity was quantified using a commercial Total Antioxidant Capacity Assay Kit (S0116, Beyotime, China) based on the ferric reducing ability of plasma (FRAP) method. Approximately 10 ml of cultures were centrifuged to harvest cell pellet. The cell pellet was resuspended by PBS and ultrasonic decomposed. After centrifugation at 12,000 × *g* for 5 min at 4 °C, the supernatant was used for antioxidant capacity measurement. For the FRAP method, the total antioxidant capacity was expressed as the concentration of the $FeSO_4$ standard solution.

Chemical analyses

Amount of CO_2 and pH. To evaluate the decomposition of n-C_{16}, the CO_2 and pH levels in the medium were measured. As CO_2 dissolved in seawater contributes H^+ and decreases the pH, thus the pH is also an indicator of n-alkane decomposition[17]. Approximately 2 ml of culture medium was injected into a 10 ml sealed glass bottle under N_2 atmosphere for CO_2 measurement. Since there was no headspace in the culture syringes, CO_2 was almost dissolved in the liquid phase. The CO_2 was quantified using gas chromatography with a BID detector (Nexis GC-2030, Shimadzu, Japan) after adding 10% H_3PO_4 (695017-100 ml, Sigma-Aldrich, USA). For pH measurement, approximately 2 ml of culture medium was detected by pH meter (FiveEasy Plus™, Mettler Toledo, Switzerland).

Extraction of n-C_{16} and analysis by GC-MS. To evaluate the consumption of n-C_{16}, the amount of n-C_{16} was determined. Due to the low solubility of n-C_{16} in seawater, three individual culture syringes were used for n-C_{16} extraction to avoid heterogeneous sampling. Before extraction, 10 μg of n-C_{20} (219274, Sigma-Aldrich, USA) dissolved in n-hexane was added to culture syringes as an internal standard to assess the recovery rate. Then, 10 ml n-hexane was added into culture syringes and syringes were shaken to mix the organic and liquid phase well. After the standing and layering process, the organic phase was sequentially transferred to a smaller tube and dried under nitrogen. Four milliliters of n-hexane was used to dissolve the residual organic matter and was then analyzed using GC-MS/MS (TSQ 9000, Thermo Fisher, USA). The n-hexadecane solution (A117437, Aladdin, China) was used as the standard to identify the peak and quantify the amount of n-hexadecane.

The mineralization ratio at each sampling point was calculated by dividing the average carbon equivalent of the net CO_2 production by the net n-hexadecane consumption, based on the three biological replicates. The average mineralization ratio was calculated by averaging the mineralization ratios from the four sampling points.

Omics analysis

Transcriptome analysis. Three of six biological replicates were used for transcriptome analysis. For each replicate, 25 ml of culture was centrifuged at 10,000 rpm for 5 min at 4 °C. The cell pellet was harvested for RNA analysis. RNA was extracted by the trizol method[34] and sequenced by Shanghai Personalbio Biotechnology Co., Ltd. (Shanghai, China). Raw reads were trimmed to remove adapters and then filtered using fastp with parameters (-w 16 -q 20 -u 20 -g -c -W 5 -3 -l 90). The rRNA reads were removed from the clean reads by ribodetecter[35]. The obtained mRNA reads were mapped to the genome of strain A28 by Burrows-Wheeler-Alignment Tool[36]. Gene reads count were calculated by featureCounts[37]. DESeq2 package was used to analyze the differentially expressed genes, with adjusted p-value < 0.05 and the absolute value of $\log_2$(fold change) ≥1.

To validate the RNA sequencing, we performed real-time quantitative reverse transcription PCR (qRT-PCR) analysis on six differentially expressed genes, using the 16S rRNA gene as an internal reference (Supplementary Methods). All qRT-PCR primers are listed in Supplementary Table 3 and the results are described in Supplementary Fig. 9.

Intracellular metabolome analysis. Six biological replicates were used for the intracellular metabolite analysis. For each replicate, 25 ml of culture was centrifuged at 10,000 rpm for 5 min at 4 °C. The cell pellet was harvested for intracellular metabolite analysis. The detail method of extraction was described in the Supplementary Methods. LC-MS/MS analyses were performed using an UHPLC system (Vanquish, Thermo Fisher, USA) with a UPLC BEH Amide column (2.1 mm × 100 mm, 1.7 μm) coupled to Orbitrap Exploris 120 mass spectrometer (Orbitrap MS, Thermo Fisher, USA). Raw data were converted to the mzXML format using ProteoWizard and processed with an in-house program, developed using R and based on XCMS, for peak detection, extraction, alignment, and integration. An in-house MS2 database (Biotree Database, Biotree Biotech CO., Ltd., China) was applied in metabolite annotation. The cutoff for annotation was set at 0.3.

Statistics and reproducibility

The statistical analyses of data and sample size are detailed in the relevant subsections of the Methods and Materials and Results and are also included in the corresponding figure legends. GraphPad Prism 10.0.0 and Adobe Illustrator 2023 were used for data analysis and visualization. Statistical significance of differences was determined using two-tailed T tests. One-way analysis of variance (ANOVA) was used for three groups. All statistical analyses were performed using non-parametric tests due to the small sample size of our experimental groups, which may not satisfy the assumptions of normality and homoscedasticity required for parametric methods. All p-values are two-sided, and a p-value < 0.05 was considered statistically significant.

Reporting summary

Further information on research design is available in the Nature Portfolio Reporting Summary linked to this article.

Data availability

All raw genomic data of *Alcanivorax xenomutans* A28, transcriptomic data and metabolomic data have been deposited to the National Omics Data Encyclopedia (NODE, https://www.biosino.org/node/index) database with project number OEP00005622. The genomic data has been deposited to eLibrary of Microbial Systematics and Genomics (eLMSG, https://www.biosino.org/elmsg/index) with accession number LMSG_G000027424.1 and NCBI databased with accession number CP169221 The raw data of genomic and transcriptomic data were also submitted to the NCBI database with accession number PRJNA1160987. The metabolomic data was also submitted to MetaboLights with project number MTBLS11036. All source data underlying the graphs and charts presented in the main figures must are provided in Supplementary Data 1.

Received: 16 October 2024; Accepted: 12 February 2025;
Published online: 16 February 2025

References

1. Board, T. R. & Council, N. R. *Oil in the Sea III: Inputs, Fates, and Effects*. (The National Academies Press, 2003).
2. Reddy, C. M. et al. The West Falmouth Oil Spill after Thirty Years: The Persistence of Petroleum Hydrocarbons in Marsh Sediments. *Environ. Sci. Technol.* **36**, 4754–4760 (2002).
3. Harvey, H. R. & Taylor, K. A. Alkane and polycyclic aromatic hydrocarbons in sediments and benthic invertebrates of the northern Chukchi Sea. *Deep Sea Res. Part II: Topical Stud. Oceanogr.* **144**, 52–62 (2017).
4. Passow, U. & Overton, E. B. The Complexity of Spills: The Fate of the Deepwater Horizon Oil. *Annu. Rev. Mar. Sci.* **13**, 109–136 (2021).
5. Fu, J., Gong, Y., Zhao, X., O'Reilly, S. E. & Zhao, D. Effects of Oil and Dispersant on Formation of Marine Oil Snow and Transport of Oil Hydrocarbons. *Environ. Sci. Technol.* **48**, 14392–14399 (2014).
6. Li, W. L. et al. Periodic and Spatial Spreading of Alkanes and Alcanivorax Bacteria in Deep Waters of the Mariana Trench. *Appl. Environ. Microbiol.* **85** https://doi.org/10.1128/AEM.02089-18 (2019).
7. Liu, J. et al. Proliferation of hydrocarbon-degrading microbes at the bottom of the Mariana Trench. *Microbiome* **7** https://doi.org/10.1186/s40168-019-0652-3 (2019)
8. Widdel, F. & Musat, F. 1–41 (Springer International Publishing, 2016).
9. Labinger, J. A. & Bercaw, J. E. Understanding and exploiting C–H bond activation. *Nature* **417**, 507–514 (2002).
10. Wang, W. & Shao, Z. Enzymes and genes involved in aerobic alkane degradation. *Front Microbiol* **4**, 116 (2013).
11. Liu, C. et al. Multiple alkane hydroxylase systems in a marine alkane degrader, Alcanivorax dieselolei B-5. *Environ. Microbiol.* **13**, 1168–1178 (2011).
12. Williams, S. C., Luongo, D., Orman, M., Vizcarra, C. L. & Austin, R. N. An alkane monooxygenase (AlkB) family in which all electron transfer partners are covalently bound to the oxygen-activating hydroxylase. *J. Inorg. Biochem* **228**, 111707 (2022).
13. Rojo, F. Degradation of alkanes by bacteria. *Environ. Microbiol.* **11**, 2477–2490 (2009).
14. Xie, Z. et al. Enhancing the Adaptability of the Deep-Sea Bacterium Shewanella piezotolerans WP3 to High Pressure and Low Temperature by Experimental Evolution under H2O2 Stress. *Appl. Environ. Microbiol.* **84** https://doi.org/10.1128/aem.02342-17 (2018).
15. Bagby, S. C. et al. Persistence and biodegradation of oil at the ocean floor following Deepwater Horizon. *Proc. Natl. Acad. Sci.* **114** https://doi.org/10.1073/pnas.1610110114 (2017).
16. Duan, J. et al. Study of residual oil in Bay Jimmy sediment 5 years after the Deepwater Horizon oil spill: Persistence of sediment retained oil hydrocarbons and effect of dispersants on desorption. *Sci. Total Environ.* **618**, 1244–1253 (2018).
17. Scoma, A. et al. Reduced TCA cycle rates at high hydrostatic pressure hinder hydrocarbon degradation and obligate oil degraders in natural, deep-sea microbial communities. *ISME J.* **13**, 1004–1018 (2019).
18. Schedler, M., Hiessl, R., Valladares Juárez, A. G., Gust, G. & Müller, R. Effect of high pressure on hydrocarbon-degrading bacteria. *AMB Exp.* **4**. https://doi.org/10.1186/s13568-014-0077-0 (2014).
19. Grossi, V. et al. Hydrostatic pressure affects membrane and storage lipid compositions of the piezotolerant hydrocarbon-degrading

Marinobacter hydrocarbonoclasticus strain #5. *Environ. Microbiol.* **12**, 2020–2033 (2010).
20. Dede, B. et al. High abundance of hydrocarbon-degrading Alcanivorax in plumes of hydrothermally active volcanoes in the South Pacific Ocean. *ISME J.* **17**, 600–610 (2023).
21. Josefien, et al. Microbial enrichment, functional characterization and isolation from a cold seep yield piezotolerant obligate hydrocarbon degraders. *FEMS Microbiol. Ecol.* **96** https://doi.org/10.1093/femsec/fiaa097 (2020).
22. Amano, C. et al. Limited carbon cycling due to high-pressure effects on the deep-sea microbiome. *Nat. Geosci.* **15**, 1041–1047 (2022).
23. Nie, Y., Liang, J., Fang, H., Tang, Y.-Q. & Wu, X.-L. Two Novel Alkane Hydroxylase-Rubredoxin Fusion Genes Isolated from a Dietzia Bacterium and the Functions of Fused Rubredoxin Domains in Long-Chain n-Alkane Degradation. *Appl. Environ. Microbiol.* (2011-10-15). https://doi.org/10.1128/AEM.00203-11.
24. Scoma, A. et al. Microbial oil-degradation under mild hydrostatic pressure (10 MPa): which pathways are impacted in piezosensitive hydrocarbonoclastic bacteria? *Sci. Rep.* **6**, 23526 (2016).
25. Holtmann, D. & Hollmann, F. The Oxygen Dilemma: A Severe Challenge for the Application of Monooxygenases? *ChemBioChem* **17**, 1391–1398 (2016).
26. Nie, Y., et al. Diverse alkane hydroxylase genes in microorganisms and environments. *Sci. Rep.* **4** https://doi.org/10.1038/srep04968 (2015).
27. Wang, W. & Shao, Z. The long-chain alkane metabolism network of Alcanivorax dieselolei. *Nat. Commun.* **5**, 5755 (2014).
28. Rose, R.-S. et al. Microbial Degradation of Plastic in Aqueous Solutions Demonstrated by CO2 Evolution and Quantification. *Int. J. Mol. Sci.* **21**, 1176 (2020).
29. Voige, W. H. Biochemical Pathways: An Atlas of Biochemistry and Molecular Biology (ed. Michal, Gerhard). *J. Chem. Educ.* **77**, 97 (2000).
30. Ahn, S., Jung, J., Jang, I. A., Madsen, E. L. & Park, W. Role of Glyoxylate Shunt in Oxidative Stress Response. *J. Biol. Chem.* **291**, 11928–11938 (2016).
31. Somero, G. N. The cellular stress response and temperature: Function, regulation, and evolution. *J. Exp. Zool. Part A: Ecol. Integr. Physiol.* **333**, 379–397 (2020).
32. Yancey, P. H. Cellular responses in marine animals to hydrostatic pressure. *J. Exp. Zool. Part A: Ecol. Integr. Physiol.* **333**, 398–420 (2020).
33. Dyksterhouse, S. E., Gray, J. P., Herwig, R. P., Lara, J. C. & Staley, J. T. Cycloclasticus pugetii gen. nov., sp. nov., an Aromatic Hydrocarbon-Degrading Bacterium from Marine Sediments. *Int. J. Syst. Bacteriol.* **45**, 116–123 (1995).
34. Rio, D. C., Ares, M., Hannon, G. J. & Nilsen, T. W. Purification of RNA Using TRIzol (TRI Reagent). *Cold Spring Harbor Protocols* **2010** https://doi.org/10.1101/pdb.prot5439 (2010).
35. Deng, Z.-L., Münch, P. C., Mreches, R. & McHardy, A. C. Rapid and accurate identification of ribosomal RNA sequences via deep learning. *Nucleic Acids Res.* **50**, e60–e60 (2022).
36. Li, H. & Durbin, R. Fast and accurate short read alignment with Burrows–Wheeler transform. *Bioinformatics* **25**, 1754–1760 (2009).
37. Liao, Y., Smyth, G. K. & Shi, W. featureCounts: an efficient general purpose program for assigning sequence reads to genomic features. *Bioinformatics* **30**, 923–930 (2014).

Acknowledgements

The authors acknowledge the crew of *TAN SUO YI HAO* Cruise TS-21. We thank the pilots of Fendouzhe HOV for their help with the sample collection. We also thank Tianyi Han and Zhou Xu for their kind assistance during experiment, Chaofan Yin for his help in results analysis, and Yu Wang for her attentive proofread for manuscript. The computations in this paper were run on the Siyuan-1 cluster supported by the Center for High Performance Computing at Shanghai Jiao Tong University. This work was supported by the National Science Foundation of China (Grant No. 42122043, 42188102, 42141003, 42306104), Research Project of of Hainan Research Institute, Shanghai Jiao Tong University (Grant No. HRSJ-ZSZX-008), National Key Research and Development Program of China (Grant No. 2023YFC2812800), Shanghai Pilot Program for Basic Research of Shanghai Jiao Tong University (Grant No. 21TQ1400201), China Postdoctoral Science Foundation (Grant No. 2023M742237).

Author contributions

H.L. and Y.Z. designed the experiments and co-wrote the manuscript. H.L. performed the experiments and statistical analysis. Y.L. analyzed the transcriptome data and improved the manuscript. Y.Z. sampled the sediment from West Philippine Basin. Y.Z. funded and supervised the project. All authors reviewed the manuscript.

Competing interests

The authors declare no competing interests.

Additional information

Supplementary information The online version contains supplementary material available at https://doi.org/10.1038/s42003-025-07728-2.

Correspondence and requests for materials should be addressed to Yu Zhang.

Peer review information *Communications Biology* thanks Nathalia Delgadillo-Ordoñez and the other, anonymous, reviewer(s) for their contribution to the peer review of this work. Primary Handling Editor: Tobias Goris. A peer review file is available.